Evolution of the three-dimensional orientation distribution of glass fibers in injected isotactic polypropylene

Luc Avérous, Jean-christophe Quantin, Alain Crespy, Dominique Lafon-Pham

Evolution of the Three-Dimensional Orientation Distribution of Glass Fibers in Injected Isotactic Polypropylene

LUC AVÉROUS, JEAN CHRISTOPHE QUANTIN, *and* ALAIN CRESPY

Ecole des Mines d'Alès
Laboratoire Matrices-Matériaux Minéraux et Organiques
30319 Alès, France

and

DOMINIQUE LAFON

Ecole des Mines d'Alès
Laboratoire Poudres, Microstructures, Macrostructures, Mines, Gisements
30319 Alès, France

The mechanical properties of fiber reinforced thermoplastics depend on the characteristics of the fibers, such as their three-dimensional orientation distribution, which is the result of the processing conditions and of the initial products before mixing. Different composites were obtained by injection of reinforced isotactic polypropylene containing 30 wt% fibers. Different size distributions of fibers were investigated. Their average lengths range from 60 to 470 μm. Specific new tools were developed by combining microscopy and image analysis to determine the microtextural characteristics of the fibers, such as their size distribution or their orientation in the matrix. Our technique allows the following of the size distribution evolution of the fibers as the composite is processed. The three-dimensional orientation of the fiber is established using the in-plane angle and the angle of inclination. The evolution of the three-dimensional orientation distribution is studied in the sample, by differentiating central and border behavior and also as a function of fiber size. It is concluded that the coupling of scanning electronic microscopy with image analysis is an interesting technique that allows the 3-D orientation of the fibers to be determined. This technique is validated by showing that the results obtained agree with those that other authors obtained on comparable materials.

INTRODUCTION

Fiber reinforced thermoplastics are increasingly used in applications where it is essential to accurately predict their composite properties. The performance of such materials is particularly dictated by the microtextural characteristics given to the matrix by the fibers. We can define microtextural characteristics as (1): the parameters of the fibers, such as their size, their shape (ratio length/diameter), and their spatial organization, determined by fiber orientation and fiber dispersion. The microtexture of a composite of given composition depends on the processing conditions and on the characteristics of the different initial products (fibers and polymer), before mixing. All these interactions can be described by the system illustrated in *Fig. 1*. It consists of the initial products, the processing conditions, the microtextural parameters, and the material properties. In order to predict material properties from initial products and processing conditions, it is necessary to analyze the different relations between each point in this system.

The particular field in which we use this approach is the analysis of the evolution of glass fiber orientation distribution in injected reinforced polypropylene. Processing conditions are fixed and controlled. The characteristics of the fibers before extrusion are varied by incorporating fibers with various size distributions into the polymer.

To determine the size distribution and three-dimensional orientation distribution of the fibers, specific procedures are developed that combine microscopy and image analysis (1–4).

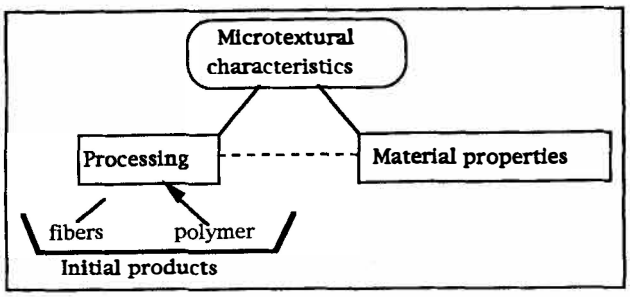

Fig. 1. Schematic presentation of the system.

The purpose of this work is to show and analyze the results obtained by the application of these image analysis methods in order to show the value of such techniques, which have been until now, rarely used in the polymer composite field. The results obtained for the evolution of the 3-D orientation distribution of the fibers can illustrate the use of such a method.

MATERIALS

Fiberglass Generation

All the fibers we used have the same diameter equal to 14 micrometers. Three different length distributions of glass fibers are obtained using different generation processes:

- a first batch of fiberglass was obtained from 4.5 mm cut thread (CFg).
- two batches of shorter glass fibers were obtained by a fragmentation process of continuous fibers. After fragmentation by pneumatic selection (Alpine ATP50 Rotoflex, Augsburg, Germany), the powder (ground glass) is eliminated leaving only glass fibers, coded SFg1.

We define the shape factor (*Fs*) as the ratio of the length to the diameter. A fiber is defined by its shape factor, $Fs > 1$. A second pneumatic selection is carried out on SFg1; the fraction containing the longest fibers is eliminated and the resulting glass fiber called SFg2. Thus, three different populations of selected glass fibers are obtained with different average lengths.

Specimen Preparation

The composites were prepared with a polypropylene matrix (Appryl 3030 MN1-Atochem-France). Its molecular weight is 325,000 Daltons. The fiber content was 30 wt%.

Processing conditions were identical for all injected specimens. A co-rotating twin-screw extruder (Clextral BC 45, Firminy, France) was used to prepare glass fiber-polypropylene pellets. An injection molding machine (Billion, Bellignat-France) with a clamping force of 90 tons was used to mold standard dumbbells. Dumbbell specimens produced have an active portion 10 mm wide and 4 mm thick (according to French standard NFT 51-034 1981). The various samples were taken from the central part of the dumbbell.

METHODS

Determination of the Size Distribution of Glass Fibers (1, 2, 4)

Most of the usual size distribution determination techniques (scattering, gravitational measurements, etc.) are not appropriate to determining the length of acicular particles such as fibers, because these methods are based on a spherical shape model. The most usual technique is therefore measuring the length of the fiber using microscopy. Semi-automatic image analyzer processes are increasingly used because of the tediousness of manual measurements (5, 6).

The most recent development has been automatic image analysis, which works more quickly and minimizes human intervention (7). We therefore developed a specific automatic technique by coupling optical microscopy and image analysis (1, 4). It is based on an individual analysis to obtain the size distribution of the fibers. The size factor for these cylindrical particles which is used in the analysis is the exodiameter, which is estimated from the maximum Feret diameter. The Feret diameter is the length of the particle projection in a determined direction on the plane.

For each analysis, a population of at least 800 fibers is treated and analyzed. Before image acquisition, fibers are carefully dispersed between two glass slides, in an appropriate dispersing solution, see *Fig. 2*. After image treatment and quantitative analysis, we obtain various types of size distribution representations and results.

—The size distribution in number, is represented by the average number length, L_n, according to the following equation:

$$L_n = \frac{\sum_i d_i \times n_i}{\sum_i n_i} \qquad (1)$$

where n_i is the number of fibers with the Feret diameter, d_i.

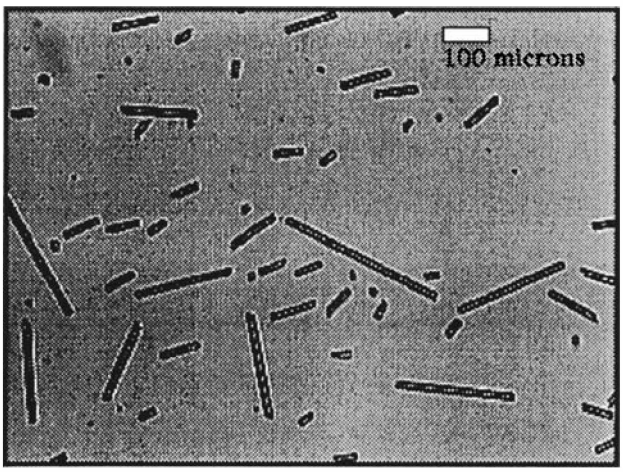

Fig. 2. Captured image of dispersed fibers between two glass slides.

—The size distribution in weight (each fiber is weighted by its length) is represented by the average weight length, L_w, as follows:

$$L_w = \frac{\sum_i d_i^2 \times n_i}{\sum_i d_i \times n_i} \quad (2)$$

The size distribution range is given by a dispersity factor: the variation coefficient (CV_n), the ratio between the standard deviation and the average length in number.

Determination of the Three-Dimensional Orientation Distribution of Fibers in the Matrix (1, 3)

To determine the orientation angles of fibers, most of the more advanced methods use their elliptical marks on a sectioned polished surface (*Fig. 3*). The three-dimensional orientation of the fiber is determined by two angles (*Fig. 4*): the inclination (θ) and the in-plane angle (ϕ), in a spherical coordinate system.

In the last decade, some authors (8–13) have followed similar approaches, but without entirely resolving the determination of both angles. Their approaches do not fully deal with the problem of 180° ambiguity on the determination of the in-plane angle. This ambiguity is due to the fact that two possible plunge senses correspond to the same elliptical mark (*Fig. 5*). Only, Clarke *et al.* (14), using a confocal scanning laser microscope, have proposed a process to determine three-dimensional orientation from two parallel optical sections of the material. Unfortunately, until now this type of microscopy has been uncommon and rather expensive.

We therefore developed an original technique by coupling scanning electron microscopy and image analysis. This technique is described in a previous paper (3). This method requires two different polished sections of the material to obtain the three-dimensional orientation distribution of the fibers in the matrix (*Fig. 6*). Grey level frames of the polished sections are taken by scanning electronic microscopy. Each image is then treated to prepare it for the quantitative analysis phase. Each frame is cleaned and a threshold is operated in order to simplify it. It is then necessary to separate touching fibers, in order to individualize and label each one. During the quantitative analysis the elliptical fiber marks are interpreted and translated into orientation results. We must be careful that fibers with irregular shaped cross section are not taken into account.

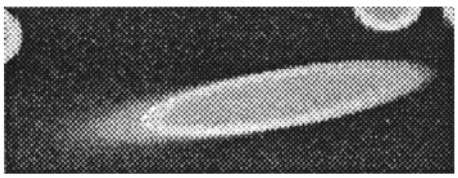

Fig. 3. Image of the elliptical mark of a fiber on a polished surface.

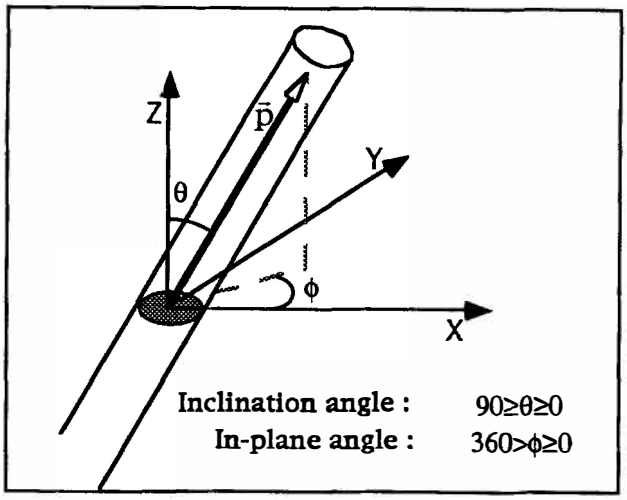

Fig. 4. Description of the orientation of a fiber.

The final orientation results could be given in two different forms.

—The second-order orientation tensor, a_{ij} (15, 16) gives a compact representation in the form of averages. The advantage of using tensor representation is that only a few data are required to describe the orientation state at any point in space. The orientation tensor is also useful in models for predicting mechanical properties.

The fiber is represented by a unit vector $\vec{p}$, which has three principal components:

$$p_1 = p_x = \sin\theta \cdot \cos\phi;\ p_2 = p_y = \sin\theta \cdot \sin\phi;\ p_3 = p_z = \cos\theta. \quad (3)$$

The second-order tensor is represented by the following equation, $a_{ij} = \langle p_i \cdot p_j \rangle$, where the brackets represent the average for the population of n studied fibers. By a discrete approach, the following equation is obtained:

$$a_{ij} = \frac{1}{n} \sum_n p_i \cdot p_j \quad (4)$$

This orientation tensor is symmetrical ($a_{ij} = a_{ji}$) and the trace equals unity ($\Sigma a_{ii} = 1$). Only five independent components are necessary to describe completely the second-order orientation tensor. In general, the three main components a_{ii}, along the three principal axes, are used.

—A very powerful representation of the orientation distribution is given by piano-spherical projections. This representation is commonly used to report orientation distribution and complex crystal textures measured by wide-angle X-ray scattering. It is called the pole figure and consists of a stereographic projection (17). Stereographic projection representations (*Fig. 7*) give not only an average measurement as in the above representations, but also the spread of the different orientation distributions. The direction rose is also constructed from the different points of the polar can-

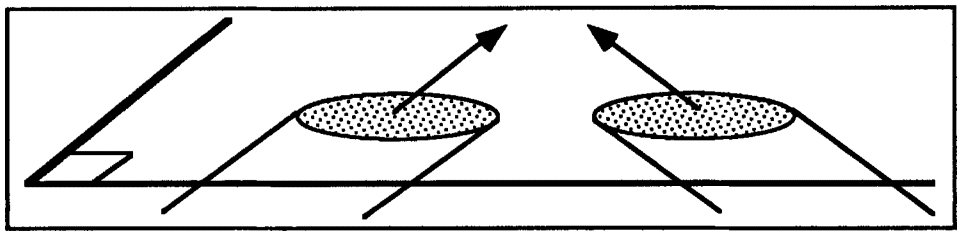

Fig. 5. Illustration of the ambiguity of the plunge sense from an elliptical mark.

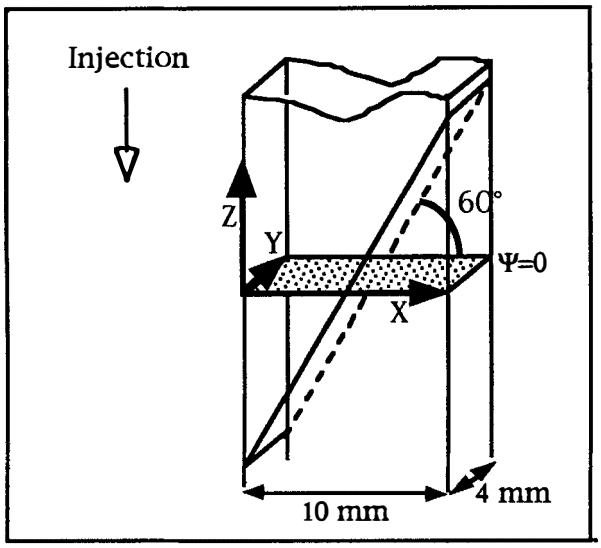

Fig. 6. Representation of the different section planes.

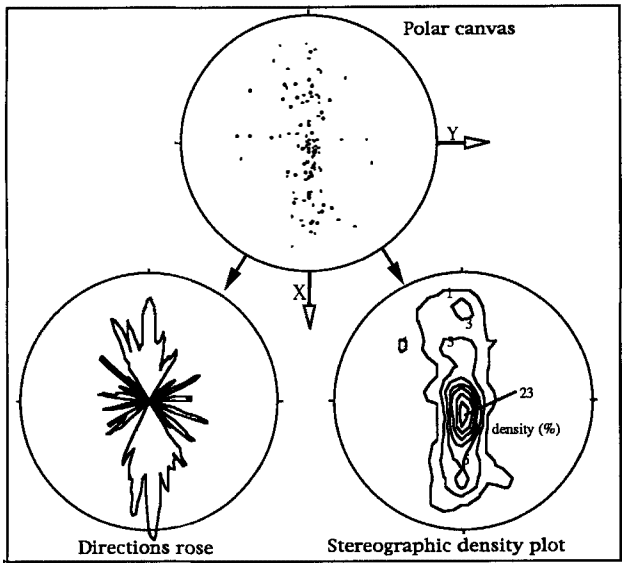

Fig. 7. Presentation of planospherical projections.

vas. Each point is translated into a unitary segment with the same plane orientation. The addition of the different segments gives the direction rose, which provides a synthetic illustration of the main fiber orientations on the plane. It shows the in-plane angle distributions, and the stereographic density plot, which gives the probability distribution of the three-dimensional orientations.

RESULTS AND DISCUSSION

Size Distribution Results

The glass fibers are separated from the matrix by pyrolysis (muffle furnace at 500°C, for 2 h. Size distribution analysis of each sample studied gives the average lengths and the dispersities of the distributions. Different size distribution results are presented in *Table 1*. The different length distributions in number are plotted on histogram displays, with logarithmic evolution (*Fig. 8*). Three different log-normal populations of fibers are detected. The populations are differentiated by their length distribution range and above all by their average length. Overall, there is a reduction in the average fiber size from CFg to SFg2.

Figure 9 (initial fibers evolutions) shows the effect of the pneumatic selection, from SFg1 to SFg2, on length distribution. It can be seen that the pneumatic selection used to eliminate the longest fiber fraction from SFg1 gives a new population of even shorter fibers, SFg2. As *Fig. 9* and *Table 1* show, this operation results in a notable reduction in the average length and a narrowing in the length distribution. The effects of grinding and processing on fiber length distribution (after extrusion and injection operations) are shown in *Fig. 9*. For short glass fibers (SFg1 and SFg2) under the chosen processing conditions, we note that fiber breakage is quite low. As noted by other authors (18, 19), this length reduction concerns principally the longest fibers, producing shorter fibers.

3D Orientation Results

Sampling Mode

Most sampling planes for orientation investigations on the injected fiber composites are established taking both core and skin behavior into account (20–22). In some cases, however, it is not possible to differentiate and identify clearly the two types of layers by microscopic observation. So, applying stereological laws, the section studied is sampled in zones of equal area. After verification of the presence of two principal symmetry axis on the plane formed by the section through

Table 1. Size Distribution Results (Average Lengths and Variation Coefficients).

	L_n (μm)	L_w (μm)	CV_n
CFg	470	700	0.69
SFg1	110	210	0.97
SFg2	60	100	0.88

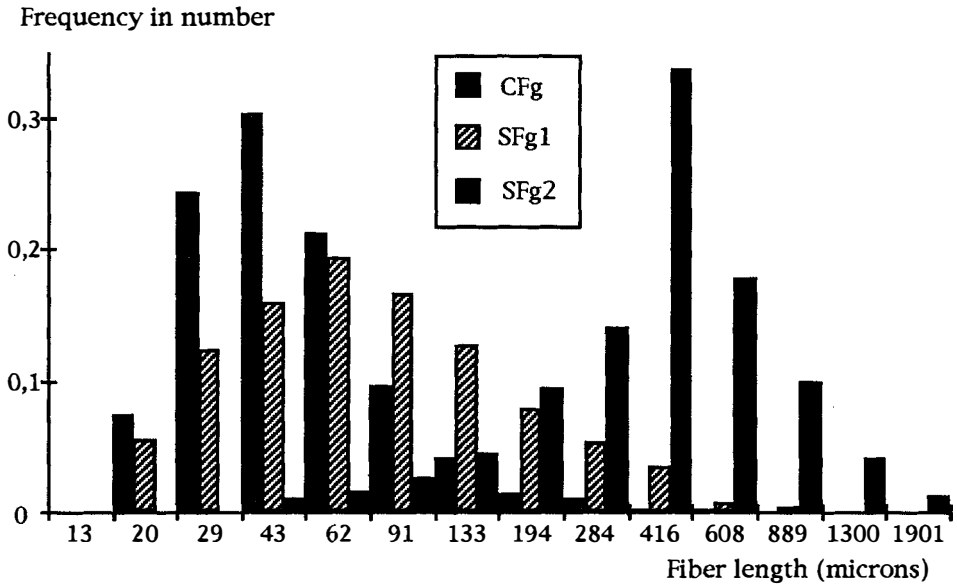

Fig. 8. Size distributions in number.

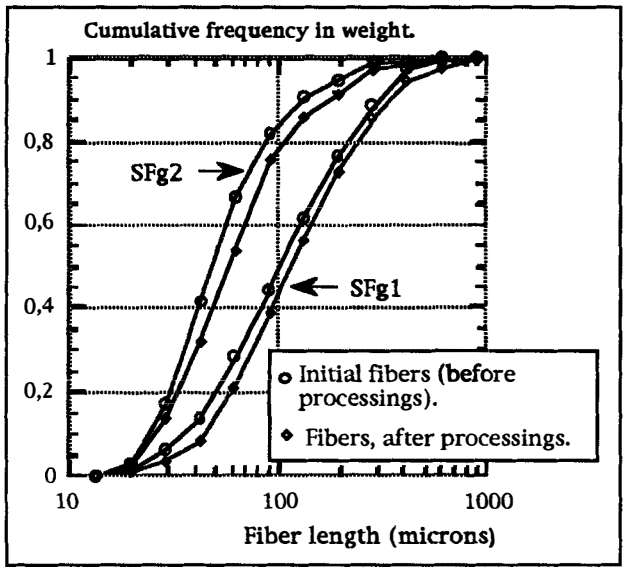

Fig. 9. Size distributions in weight. Cumulative presentation.

the central part of the injected dumbbell (1), investigation is limited to a quarter of this surface. This surface is described by ten different sampling zones. On the plane perpendicular to the injection direction ($\Psi = 0°$), square zones of 1×1 mm^2 are defined (*Fig. 10*). Each zone can be considered independently, one can distinguish six border zones on the specimen (principal border, along the X axis, and secondary border, along the Y axis) and four other central zones.

Fiber Inclination

In border zones, fibers are mainly perpendicular to the section plane. On the stereographic density plots, a high central peak is noticeable. Where the shear is more severe during the mold filling, close to the mold surface, fibers are principally parallel (20–25). This effect is clearly shown by the high values of the a_{33} tensor component (*Fig. 11*) and the high central peak on stereographic density plots (*Figs. 12* and *13*). These results are in agreement with Tadmor's fountain flow mechanism for unfilled polymers (26) and with Jeffery's model describing the movement of an ellipsoidal body in a shear flow (27).

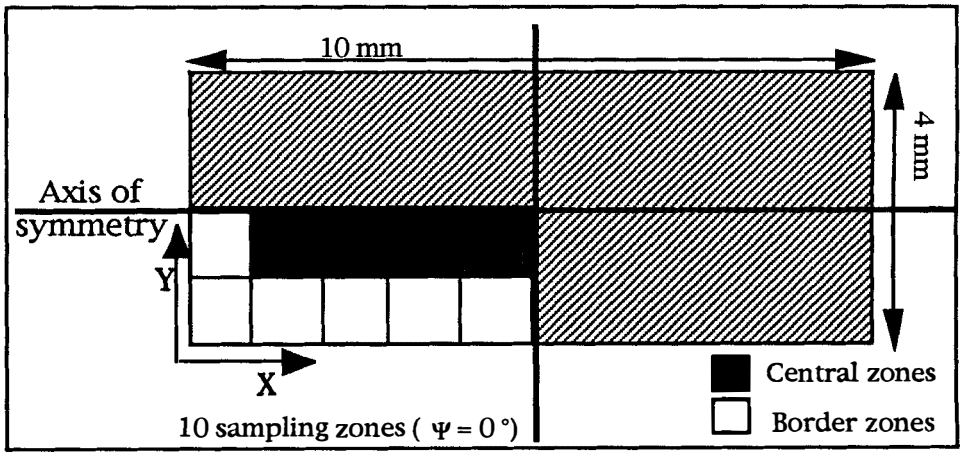

Fig. 10. Principal samplings zones and symmetry axis.

a11 (axis X)		a22 (axis Y)		a33 (axis Z)	
0,20	0,08	0,03	0,08	0,77	0,85
0,19	0,09	0,01	0,07	0,80	0,84
0,16	0,08	0,01	0,02	0,83	0,89
0,17	0,30	0,00	0,03	0,83	0,68
0,33	0,33	0,00	0,01	0,67	0,65

CFg results.

0,05	0,03	0,07	0,10	0,89	0,87
0,07	0,12	0,03	0,12	0,90	0,76
0,11	0,25	0,02	0,06	0,88	0,69
0,09	0,27	0,02	0,05	0,89	0,67
0,15	0,30	0,03	0,04	0,82	0,66

SFg1 results.

0,19	0,16	0,04	0,08	0,78	0,76
0,13	0,09	0,03	0,21	0,84	0,70
0,16	0,40	0,06	0,11	0,78	0,50
0,35	0,57	0,03	0,05	0,61	0,39
0,44	0,59	0,01	0,02	0,54	0,38

SFg2 results.

Fig. 11. Presentation of the tensor component data, for each zone and each product.

On the other hand, for more central zones, the shear is smaller and the velocity vector greater. In this case, the fibers tend to be positioned more transversely in the direction of injection. When fiber inclination increases, a decrease and a shifting of the central peak on the stereographic density plots are observed. The summit tends to spread on both sides around the center of the plot. Going away from the secondary border (border parallel to the *Y* axis) towards the center, there is a decrease in the a_{33} value; the fiber inclination increases. In the center, we note that the fiber inclination is inversely proportional to the fiber size, mainly because the smaller fibers are more mobile as the flow front advances during the filling of the mold. The averages of the orientation tensor component a_{33} increase from SFg2 to CFg. Shorter fibers tend to stand perpendicularly to the injection flow, in the core of the injected part. These results are in total agreement with Bailey and Rzepka's studies (20) concerning fiber behavior inside the flow as a function of the particle size.

In-Plane Fiber Orientation

The orientations rose allows the representation of the in-plane orientation distribution to be clarified. This graphic representation is reinforced by tensor component values, principally a_{11} and a_{22}.

In border zones, in-plane orientation tends to be parallel to the principal border. We can note that the value of a_{11} is higher than a_{22}. Towards the center, along the *X* axis, the a_{11} tensor component increases. The further from the secondary wall, the more the fibers are orientated parallel to the principal wall along the *X* axis. In-plane orientations in the two zones close to the secondary wall are confused due to the influence of both borders.

For central zones, we note that the further away from the secondary border, the more the fibers are orientated progressively parallel to the *X* axis (*Figs. 15* and *16*). The influence of the principal wall is predominant. This is shown by an increase in a_{11} and a decrease in a_{22} values. The shorter the fibers are, i.e. mobile in the flow, the greater is the effect. By analyzing stereographic density plots, a dissymmetry in the 3D orientation distribution is detected. We can notice that the density extrema are shifted toward the center, along the *X* axis. This is due to the rheology of the system and this is in agreement with mold filling models, given e.g. in the simulations of Advani and Tucker (26) or Baraldi *et al.* (24).

The in-plane orientation ϕ and the symmetric angle $\phi + 180°$ do not have the same probability. In our case, the in-plane angle ϕ close to 0° is more frequent than the 180° angle. This is due to the curvature of the advancing front during mold filling (*Fig. 17*), which favors a particular plunge sense.

We observe that, for the same fiber concentration, on a polished section, the shorter the fibers are, the

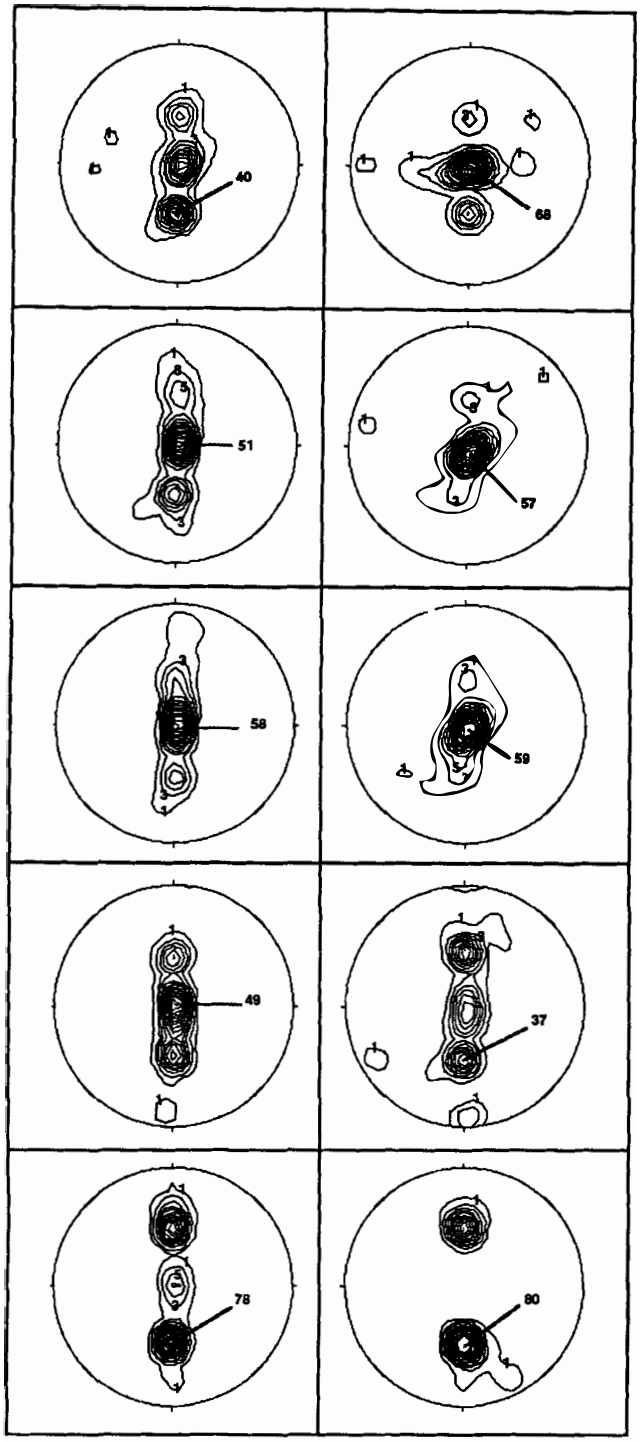

Fig. 12. Stereographic density plots of CFg.

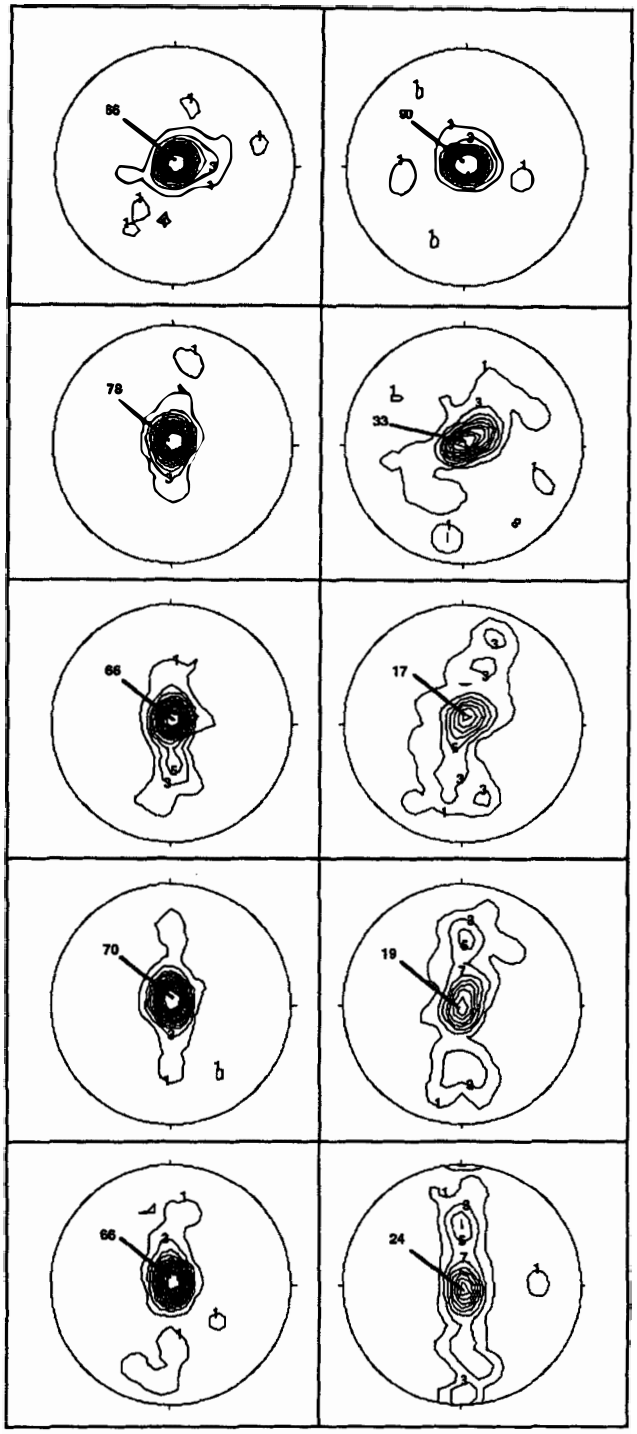

Fig. 13. Stereographic density plots of SFg1.

more fiber ends there are on the frame, and there are fewer elliptical fiber marks. Non-elliptical particles, like fiber ends, cause bad particle separation in the automatic segmentation process used during the image treatment phase. They are, therefore, rejected from the orientation quantification. This results in the SFg2 stereographic ploting (*Fig. 14*) being of poorer quality. So, the uncertainty in the orientation determination measurements tends to increase inversely with the size under analysis.

The reproducibility of the results have already been demonstrated (1). In addition, our results agree with those of other authors working in the fiber orientation field (20–22, 24, 25). The method we propose for the determination of the 3D orientation of fibers in injected reinforced polymers therefore appears a valid one.

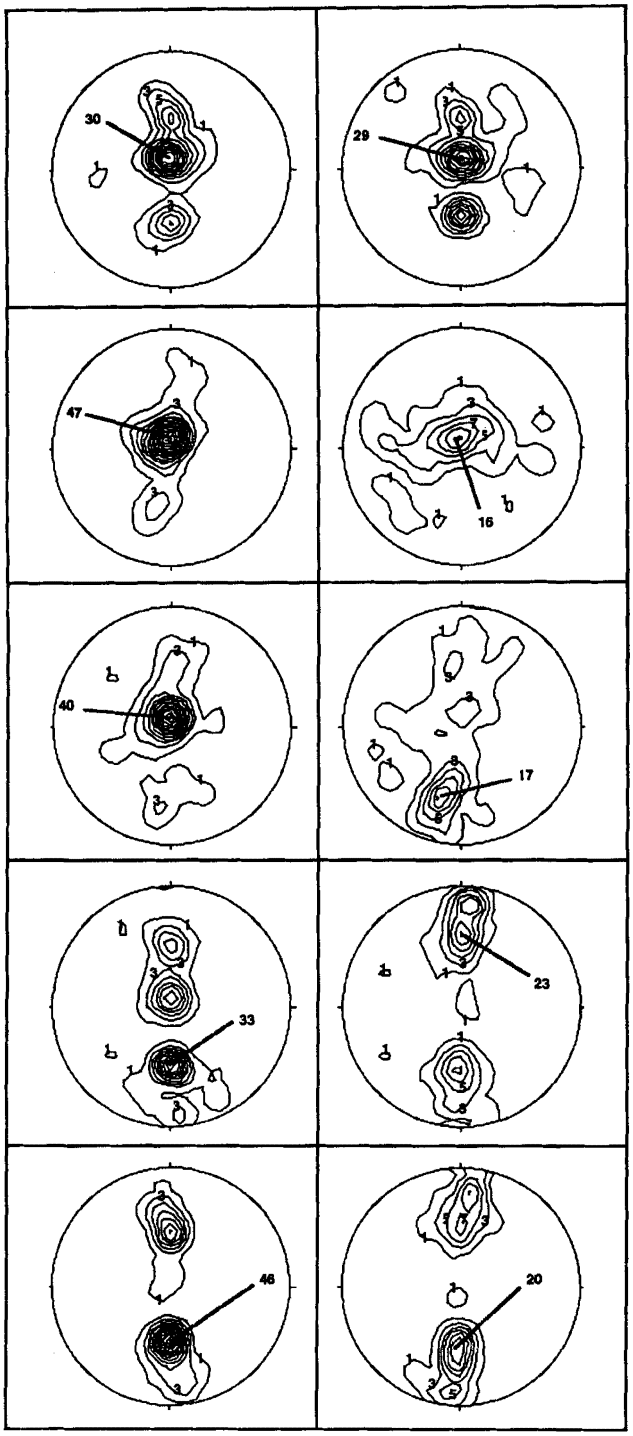

Fig. 14. Stereographic density plots of SFg2.

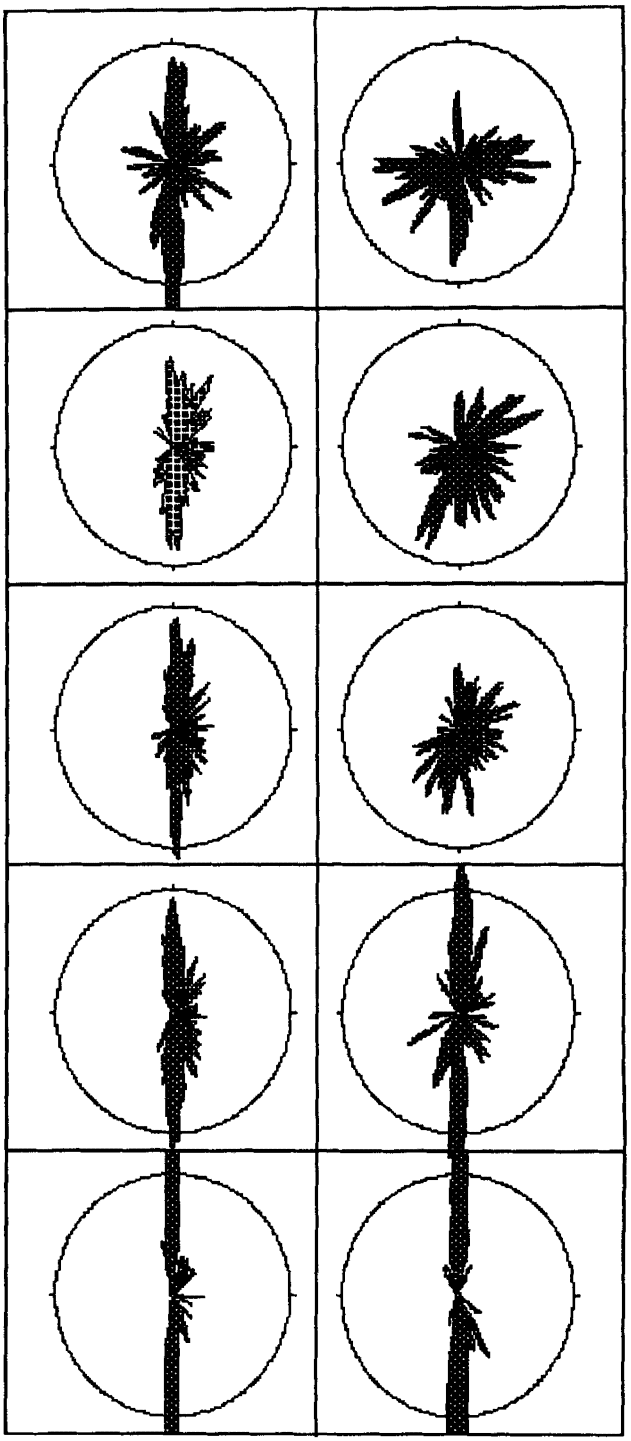

Fig. 15. Directions rose of CFg.

CONCLUSIONS

This paper shows essentially the great usefulness of image analysis techniques, such as 3D orientation determination, in the precise determination of some material characteristics given by the fibers to the polymer composite. An original tool which we developed, uses scanning electronic microscopy. It allows us to investigate the distribution of three-dimensional orientations on various glass fiber reinforced polypropylenes, characterized by different incorporated fiber sizes. The different length distributions are determined by using a specific method which consists of coupling image analysis and optical microscopy in order to be able to measure precisely the size of the fibers in the various injected materials analyzed. We verified that the composites are different in terms of their fiber lengths even after processing.

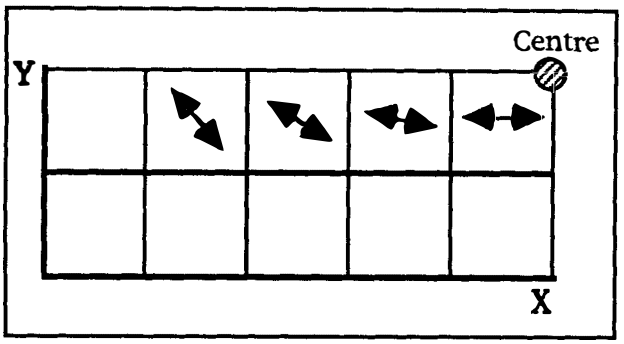

Fig. 16. Evolution of in-plane orientations on central zones.

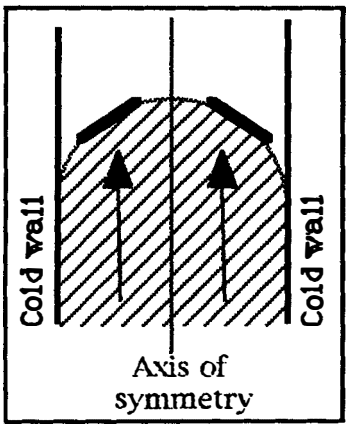

Fig. 17. Illustration of the curvature of the advancing front.

For the chosen sampling mode and processing conditions, we followed the orientation of fibers in the sample, by differentiating central (core) and border (skin) behavior using different types of representation of the results. The evolution of this behavior according to fiber length is also investigated. These results are in accord with different authors' results concerning fiber mobility and the corresponding orientation in the flow during the filling of the mold. Moreover the data provided by our technique will be very useful to model the mechanical behavior of our materials.

REFERENCES

1. L. Avèrous, thesis, Ecole des Mines de Paris (1995).
2. L. Avèrous, D. Lafon, J. C. Quantin, A. Benhassaine, and A. Crespy, *Proc. MOFFIS 93, Namur-Belgium*, 293 (1993).
3. L. Avèrous, J. C. Quantin, D. Lafon, and A. Crespy, *Acta Stereol.*, **14/1** (1995).
4. L. Avèrous, J. C. Quantin, D. Lafon, and A. Crespy, *Int. J. Polym. Anal. and Charact.*, **1,** 339 (1995).
5. L. C. Sawyer, *Polym. Eng. Sci.*, **19,** 377 (1979).
6. T. Allen, in *Particle Size Measurement*, Chapman and Hall, New York (1990).
7. H. Talbot, thesis, Ecole des Mines de Paris (1993).
8. S. Fakirov and C. Fakirova, *Polym. Compos.*, **6,** 41 (1985).
9. G. Fischer and P. Eyerer, *Polym. Compos.*, **9,** 297 (1988).
10. A. Vaxman, M. Narkis, A. Siegmann, and S. Kenig, *J. Mater. Sci., Letters*, **7,** 25 (1988).
11. G. Fischer, P. Schwarz, U. Mueller, and U. Fritz, *Adv. Polym. Technol.*, **10,** 135 (1990).
12. S. Toll and P. O. Andersson, *Composites*, **22,** 298 (1991).
13. P. J. Hine, R. A. Duckett, N. Davidson, and A. R. Clarke, *Compos. Sci. Technol.*, **47,** 65 (1993).
14. A. R. Clarke, N. Davidson, and G. Archenhold, *J. Microscopy*, **171,** 69 (1993).
15. S. G. Advani and C. L. Tucker, *SPE ANTEC Tech., Papers*, **31,** 1113 (1985).
16. S. G. Advani and C. L. Tucker, *J. Rheol.*, **31,** 751 (1987).
17. C. Whiston, in *X-Ray Methods*, John Wiley and Sons, Chichester, United Kingdom (1987).
18. M. Arroyo and F. Avalos, *Polym. Compos.*, **10,** 117 (1989).
19. D. Wall, *Polym. Compos.*, **10,** 98 (1989).
20. R. Bailey and B. Rzepka, *Int. Polym. Process.*, **1,** 35 (1991).
21. P. A. O'Connell and R. A. Duckett, *Compos. Sci. Technol.*, **42,** 329 (1991).
22. J. P. Tancrez, thesis, Univ. of Lille, France (1994).
23. M. R Kamal, L. Song, and P. Singh, *Polym. Compos.*, **7,** 323 (1986).
24. M. Vincent and J. F. Agassant, "Predicting Fiber Orientation in Injection Molding" in *Two-phase Polymer Systems*, Chap. 11, L. A. Utracki eds., Hanser Publishers, New York (1991).
25. U. Baraldi, J. F. Lucarelli, and A. Fouarge, *J. Polym. Eng.*, **11,** 1 (1992).
26. Z. Tadmor, *J. Appl. Polym. Sci.*, **18,** 1753 (1974).
27. G. B. Jeffery, *Proc. Roy. Soc.*, **A102,** 161 (1922).
28. S. G. Advani and C. L. Tucker, *Polym. Compos.*, **11,** 164 (1990).